Design of a AB_5-metal hydride cylindrical tank for hydrogen storage

Yuanlu Li[1], Erika Teliz[1,2], Fernando Zinola[1], Verónica Díaz[2*]

[1]*Facultad de Ciencias, Grupo Interdisciplinario Ingeniería Electroquímica (GIIE) Universidad de la Republica (UdelaR), Iguá 4223, CP 11400, Montevideo,Uruguay*

[2]*Facultad de Ingeniería, Grupo Interdisciplinario Ingeniería Electroquímica (GIIE) Universidad de la Republica (UdelaR), J. Herrera y Reissig 565,CP11300, Montevideo,Uruguay*

**Corresponding author: verodiaz@fing.edu.uy*

Abstract

Hydrogen storage in metal hydrides presents distinct challenges which encourage the study of effective heat management strategies. Hydrogen absorption in metal hydrides is an exothermic reaction, consequently the generated heat must be removed effectively to achieve the desired performance. This work presents a mathematical model describing the adsorption of hydrogen in La $Ni_{4.7}Co_{0.3}$ metal hydride as a storage material. Heat and mass transfer effects are modeled in detail. The effect of heat transfer coefficient is also estimated. Besides, a heat transfer fluid for cooling is incorporated to the model. The problem is mathematically formulated presenting a numerical simulation of a design of a cylindrical tank for hydrogen storage. The alloy is studied by using pressure-composition-temperature (PCT) curves which are carried out at different temperatures. Thermodynamic parameters and hydrogen storage capacity are determined. For isotherm's kinetics, the Jonhson-Mehl-Avrami-Kolomogorov (JMAK) model is used, from which the kinetic constant of the hydriding process is determined.

***Keywords**:* Metal hydrides; Hydrogen; Energy storage; Heat transfer; Absorption; Kinetic model

1 Introduction

Nowadays, there is a noticeable interest in the search of clean and renewable energy, especially those associated with solar and wind sources. However, it is worthwhile noticing that these sources are intermittent so their power integration to the electric grid is a great challenge [1-4].

In other words, the development of appropriate energy storage technology is required to utilize renewable energy effectively. In the last decade, many researchers focused on solve this problem associated with the shift between demand and energy generation [5-8]. Among several options found by researchers, the hydrogen based renewable

energy storage system is one of the best ones. Hydrogen has several attractive attributes as an energy carrier in the near future. It is worthwhile noticing that a global conversion from fossil fuels to hydrogen requires the removal of many barriers imposed along the stages involved in hydrogen knowhow. One of the main problems is the storage [9-11].

Conventional storage methods listed in Table 1 such as gas compression and liquefaction have many disadvantages [9-10]. Storing hydrogen in metal hydrides beds appears to be a promising method of hydrogen storage in the near future [12]

Table 1. Categorization of forms of hydrogen storage

Category	Subcategory	Volumetric density	Gasometric density	Pressure (bar)	Temperature (ºC)
		(**kg**H_2/m^3)	(%*mass*)		
Gas	Pressure Cylinder	33	13	800	25
Liquid	Termo type Dewar	71	100	1	-252
Solid	Metal hydrides	150 max	2	1	25
Solid	Physisorption	20	4	70	-208
Solid	Complex Hydrides	150	18	1	25
Solid	Chemical reaction with water	>100	14	1	25

Metal hydrides are very promising materials for hydrogen storage because hydrogen absorption and desorption can be done at room temperatures. Although the volumetric storage capacity of hydrogen is high, they have a low gravity storage capacity, but this is not an inconvenience for parking applications compared to mobile ones.

Metal hydrides are characterized by the following reversible reaction (eq 1), where ΔH is the heat of reaction.

$$xM + \frac{y}{2}H_2 \rightleftarrows M_xH_y + \Delta H \qquad (1)$$

Metal hydrides absorb hydrogen releasing heat and to desorb hydrogen, heat must be supplied. These exothermic and endothermic heats can be useful in other applications such as heating and air conditioning applications. Therefore, heat management in the storage tank is very important because it affects the absorption and desorption rate of hydrogen. [13-16]

Heat absorbed and released during the hydriding and dehydration process is a critical point in the design. As the absorption reaction is an exothermic process and desorption is endothermic, the design of the heat exchange system is a fundamental point in the storage performance. The hydrogen storage system is one of the crucial components of the total system. The purpose of the metal hydride tank is to absorb and desorb hydrogen for storage and simultaneously use the heat of reaction for air conditioning. [4]

Many researchers have their focus on the mathematical modeling of hydrogen storage in metal hydride beds over the last decade. Jemni and Nasrallah [17-19] reported a theoretical study of mass and heat transfer processes in a metal hydride reactor. Kaplan [12] developed a mathematical model to describe hydrogen absorption in a porous La metal hydride bed and investigated the hydrogen storage process including the full momentum balance equation, which is important in presence of large pressure gradients. On the other hand, Nakagawa et al. [20] presented a bidimensional model for the transitory state of heat and mass transfer within a metal hydride bed and Askri et al. [21] studied the effect of radiate heat transfer in La and Mg metal hydride beds.

The hydrogen storage in metal hydrides presents distinct tasks which motivate the need for effective heat management strategies [22-24]. This work presents a mathematical model describing the adsorption of hydrogen in a La $Ni_{4.7}Co_{0.3}$ AB5 type metal hydride bed. Heat and mass transfer effects are modeled in detail. The effect of heat transfer coefficient is also estimated. Then, a cooling medium model is incorporated with the hydrogen storage model. The problem is mathematically formulated presenting a numerical simulation of a design of a cylindrical tank for hydrogen storage. In the experimental section, $LaNi_{4.7}Co_{0.3}$ alloy is studied by using pressure-composition-temperature (PCT) curves at different temperatures. Thermodynamic parameters and hydrogen storage capacity are determined. For isotherm's kinetics, the Jonhson-Mehl-Avrami-Kolomogorov (JMAK) model is used, from which the kinetic constant of the hydriding process is determined.

2 Experimental procedures

2.1 Synthesis of alloys

A $LaNi_{4.7}Co_{0.3}$ alloy was synthesized by arc melting under high purity argon from pure metallic ingots of each component. The resulting alloy "button" was re-melted twice to ensure the sample homogeneity.

2.2 Gaseous phase characterization: PCT curves

Gaseous phase hydrogen storage characterization of the alloy was carried out by PCT isotherm measurement using an automatically controlled Sievert's apparatus. The sample (1 g of alloy) was put into a cylindrical reactor with controlled temperature in every experiment. Before PCT analysis, each sample was first activated by a routine of absorption / desorption cycles at room temperature for 12 hours. PCT isotherms at 298, 313 and 328 K were then measured until H_2 pressure of 8 Bar.

Based on the PCT curves, thermodynamic parameters of hydrogen absorption at a particular hydrogen concentration can be calculated from Van't Hoff (equation 2) [25]

$$Ln\,(P) = \frac{\Delta H^{o}}{R}\frac{1}{T} - \frac{\Delta S^{o}}{R} \qquad (2)$$

2.3 Kinetic models JMAK

JMAK (Jonhson-Mehl-Avrami-Kolomogorov) models [26] are generally used to describe the hydrogen absorption process, which can be simplified as

$$\xi = 1 - exp\,(-kt^{n}) \tag{3}$$

where ξ is the reaction fraction, k is the rate constant of the reaction, and n is the Avrami exponent. This expression can be linearized, so that the exponent can be obtained directly from the slope of the fit line, k can be obtained from Y- interception at its corresponding temperature.

$$\ln\,(-\ln\,(1-\xi)) = n\ln t + \ln k \tag{4}$$

The equipment EVA-5 (nunca dice lo que es) which is designed to measure hydrogen absorption by solid absorbent materials automatically saves the pressure evolution information over time. The initial pressure for all experiences is 5 bars. With this information it is possible to calculate the fraction of reaction advance by means of the following equation:

$$\xi = \frac{P_{initial} - P_t}{P_{initial} - P_{final}} \tag{5}$$

Applying Arrhenius's law:

$$k = k_{iso}\exp(-\frac{E_0}{RT}) \tag{6}$$

This expression also can be linearized.

$$\ln k = -\frac{E_0}{R}\frac{1}{T} + lnk_{iso} \tag{7}$$

Where E_o is the activation energy, k_{iso} is Arrhenius constant, and T the temperature. Therefore, performing a linear regression with kinetic constants at different temperatures it is possible to obtain from the slope, the activation energy of the process.

3. Mathematical modeling

Mathematical models discussed in this paper consist of a cylindrical metal hydride with an internal cooling heat exchange tube and without heat exchange tube. The metal hydride tank is filled with the studied alloy and the heat transfer fluid flows through a lineal central tube of the heat exchanger to remove the exothermic heat during the absorption process. Energy balance and mass balance differential equations

are imposed with specified initial and boundary conditions detailed in the resulting section.

The following equations are included in a program with Octave while simulating the metal-hydrogen reaction process.

3.1 Equilibrium pressure

To begin with, the reactor is in equilibrium with hydrogen so P_{eq} can be calculated from Van't Hoff (equation 2).

$$P_{eq} = \exp\left[\frac{\Delta H}{R}\frac{1}{T} - \frac{\Delta S}{R}\right] \tag{8}$$

Where ΔH and ΔS were obtained from the PCT experiment.

3.2 Mass absorption rate

The mass rate of hydrogen absorbed by the metal hydride, m per unit of time and per unit of porous medium volume, expressed as equation (9), is directly related to the reaction rate [16].

$$m = k_{iso}\exp^{-\frac{E_0}{RT}} ln\frac{P_g}{P_{eq}}\Delta\rho_s(1-\xi) \tag{9}$$

where k_{iso} and E_0 were obtained from Arrhenius adjustment and were just defined, Pg is the hydrogen supply pressure and ξ can be estimated from equation (3) [26]. $\Delta\rho_s$, defined as $\Delta\rho_s = \rho_{ss} - \rho_{s0}$ is the fictitious density increment owing to the hydrogenation process [27], which is directly related to the capacity of hydrogen storage. ρ_{ss} is the effective density of solid at saturation and ρ_{s0} is the effective density of solid without any hydrogen absorption. The fictitious density increment can be expressed as:

$$\Delta\rho_s = \rho_{metal}\,(1-\varepsilon)\,wt\,\% * 0.01 \tag{10}$$

where ε is the porosity and wt% is the hydrogen storage capacity in terms of weight percent which is defined as [28]:

$$wt\,\% = \frac{m_{H2}}{ma}\,100\% \tag{11}$$

being m_{H2} the hydrogen mass absorbed and ma the mass of the alloy.

3.3 Energy balance

The first law of thermodynamics addresses total energy, a steady-state condition must prevail such that there will be no change in the amount of thermal and mechanical energy stored in the control volume. Thermal and

Mechanical Energy Equation at an Instant (t) can be expressed as equation (12) [29].

$$\dot{\mathrm{E}}_{st} = \frac{\delta E_{st}}{\delta t} = \dot{\mathrm{E}}_{in} - \dot{\mathrm{E}}_{out} + \dot{\mathrm{E}}_{g} \qquad (12)$$

Where $\dot{\mathrm{E}}_{st}$ is the stored thermal and mechanical energy at t time; $\dot{\mathrm{E}}_{in}$ and $\dot{\mathrm{E}}_{out}$ are thermal energy transport across the control surfaces at *t* time, that is, the inflow and outflow terms respectively; $\dot{\mathrm{E}}_{g}$is the thermal energy generation at the same time.

Thermal energy generation can be calculated as the equation (13), where s is the heat source term that is released by hydrogen absorption during the reaction; M_{H2} is the molecular weight of hydrogen gas; *V* is the volume of alloy and ρ_{s0} is the effective density of solid without any hydrogen absorption: [4]

$$s = \mathrm{m}\frac{\Delta H}{\mathrm{M}_{H_2}} \qquad \dot{\mathrm{E}}_{\mathrm{g}} = s * \rho_{s0} V \qquad (13)$$

The heat transfer fluid flows through the heat exchanger inside the reactor bed, so the convective condition can be expressed [4]:

$$q_{\mathrm{out}} = -\mathrm{k}\frac{\mathrm{dT}}{\mathrm{dr}} = U(T_{\mathrm{m}} - T_{\mathrm{cool}})$$

$$\dot{\mathrm{E}}_{\mathrm{out}} = q_{\mathrm{out}}\mathrm{A} \qquad (14)$$

Where T_{m} is the average temperature of cylinder and *U* is the global heat transfer coefficient. A is the area of heat exchange. Assume ambient temperature and coolant temperature are the same as T_{cool} which are supposed constantly during the process.

For the estimation of natural convection h_2, Churchill and Chu [30] have recommended a single correlation (see equation 15) for a wide range of Rayleigh numbers:

$$\overline{Nu_D} = h_2\frac{L}{k} = \left\{0.6 + \frac{0.387 * Ra^{\frac{1}{6}}}{\left[1+\left(\frac{0.559}{Pr}\right)^{\frac{9}{16}}\right]^{\frac{8}{27}}}\right\}^2 \qquad Ra \leq 10^{12} \qquad (15)$$

Where Prandtl number is:

$$Pr = \frac{\mu Cp}{k} = \frac{v}{a} \qquad (16)$$

And Rayleigh's number is defined as:

$$Ra_L = Gr_L * Pr = \frac{g\beta(T_s - T_\infty)L^3}{v\alpha} \quad (17)$$

Where: L is the length of geometry; T is the absolute temperature; g is the gravitational acceleration; v is the kinematic viscosity; α is the thermal diffusivity and β is the expansion coefficient

α
Forced convection is designed by using water as refrigeration. h_1 is estimated with Eagle-Ferguson (equation 18) [29]

$$h_1 = 150(1 + 0.011 \cdot T_m)\frac{u^{0.8}}{d^{0.2}} \quad (18)$$

Where: h_1 = film coefficient of heat transfer in BTU/(hr · ft² · °F); Tm = arithmetic mean temperature of water (° F); u = mean speed of water (ft / s); d = inside diameter of the tube (in); The global heat transfer coefficient U is the same as h_1 for the cylinder without heat exchange tube, while U for the design with inner tube can be calculated as equation (19):

$$U = h_1 + \frac{h_2 r_2}{r_1} \quad (19)$$

where r_1 is the radium of inner tube and r_2 is the radium of cylinder.
In this hydrogen storage system $\dot{E}_{in}$ is zero and from the energy balance equation we can obtain equation (20):

$$\frac{\delta T_{\mathrm{m}}}{\delta t} = \frac{\mathrm{s}}{C_{\mathrm{pef}}\,\rho_{s0}} - \frac{\mathrm{UA}}{VC_{\mathrm{pef}}\,\rho_{s0}}(T_{\mathrm{m}} - T_{\mathrm{cool}}) \quad (20)$$

where the effective specific heat can be expressed as:

$$(\rho C_p)_{ef} = \varepsilon\,(\rho C_p)_g + (1 - \varepsilon)(\rho C_p)_m \quad (21)$$

being ρ_g and ρ_s the hydrogen density and the solid density respectively, C_{pg} and C_{pm} are the specific heat of hydrogen and material respectively and ε is the porosity.

In the energy balance we can assume $L \gg r_0$, so the losses of heat generated during the absorption reaction in the axial direction can be neglected. The Fourier equation can be simplified to the following form:

$$\frac{1}{r}\frac{\partial}{\partial r}\left(k_{ef} r \frac{\partial T}{\partial r}\right) + s = \rho c_p \frac{\partial T}{\partial t} \quad (22)$$

Effective thermal conductivity is given by:

$$k_{ef} = \varepsilon\, k_g + (1 - \varepsilon)k_m \quad (23)$$

For steady-state condition, surface temperature remains at a fixed value T_s .The temperature distribution is determined analytically assuming steady state and constant conductivity. The temperature profile of the solid cylinder is the heat equation results in Eq. (24): y cuales son las condiciones de iniciales?

$$T_{(r)} = \frac{s \cdot r_0^2}{4 \cdot k_{ef}}\left(1 - \frac{r^2}{r_0^2}\right) + T_s \quad (24)$$

where the maximum temperature can be obtained at r=0.
The average temperature can be calculated by the following integration:

$$T_{av} = \frac{\int_0^{r_0} T_{(r)} \rho 2\pi r L dr h}{\int_0^{r_0} \rho 2\pi r L dr h} = \frac{s \cdot r_0^2}{8 \cdot k_e} + T_s \quad (25)$$

The temperature profile which has the inner tube refrigeration also can be obtained by solving the differential equation at the steady-state condition:

$$T_{(r)} = \frac{s}{4 \cdot k_e}(r_1{}^2 - r^2) + \frac{\left[(T_{s_1} - T_{s_2}) + \frac{s}{4 \cdot k_e}(r_1{}^2 - r_2{}^2)\right] ln\left(\frac{r}{r_1}\right)}{ln\left(\frac{r_1}{r_2}\right)} + T_{s_1} \quad (26)$$

where T_{s1} is the inner superficial temperature and T_{s2} is the temperature of outside surface. The maximum reactor temperature can be found at a radio value determined in equation (27)

$$r_{Tmax} = \sqrt{\frac{(T_{s_1} - T_{s_2}) 2k}{s ln\left(\frac{r_1}{r_2}\right)} + \frac{(r_1{}^2 - r_2{}^2)}{2 ln\left(\frac{r_1}{r_2}\right)}} \quad (27)$$

The average temperature at this design is:

$$T_{av} = T_{s_1} + \frac{s(r_1{}^2 + r_2{}^2)}{8k_e} + \frac{s(r_2{}^2 - r_1{}^2)}{8k_e ln\left(\frac{r_1}{r_2}\right)} + \frac{r_2{}^2 (T_{s2} - T_{s_1})}{(r_2{}^2 - r_1{}^2)} + \frac{(T_{s2} - T_{s_1})}{2 ln\left(\frac{r_1}{r_2}\right)} \quad (28)$$

During the process, hydrogen and air are considering as ideal gas and the temperature change of cooling water is negligible.

$$\rho_g = \frac{P_g M}{RT} \quad (29)$$

The properties of hydrogen, air and water used in this simulation are listed in Table 2

Table 2. Hydrogen air and water properties

Properties	Value	Reference
Molecular weight M_{H2}	2 g/mol	
Gas constant R	8.314 J/mol K	
Specific heat of H_2 Cp_{H2}	0.01489 J/g K	[22]
Thermal conductivity of hydrogen k_{H2}	0.24 W/m K	[27]
Thermal conductivity of k_{air}	0.0263 W/m K	[31]
Air density ρ_{air}	83.8 g/m^3	[31]
Air kinematic viscosity ν_{air}	0.00001589 m^2 /s	[31]
Thermal diffusivity α	0.0000225 m^2 /s	[31]
Prandtl number Pr	0.707	[31]
Specific heat of water Cp_{water}	4.182 J/g K	
Water density $\rho_{wat\,er}$	997000 g/m^3	

The properties of the studied alloy (La $Ni_{4.7}Co_{0.3}$) used in the present simulation are listed in Table 3.

Table 3. Properties of the studied alloy.

Properties	Value	Reference
Activation energy E_a	34.3 kJ/mol	
Reaction constant k_{iso}	16662 s $^{-1}$	
Thermal conductivity k_m	3.2 W/m K	[27]
Effective thermal conductivity k_{ef}	1.6 W/m K	[22]
Effective specific heat Cp_{ef}	0.419 J/g K	[22]
Metal density ρ_m	7784000 g/m^3	
Effective density of solid ρ_{s0}	3892000 g/m^3	
Effective density of solid at saturation ρ_{ss}	3931000 g/m^3	
Porosity ε	0.5	
Reaction enthalpy ΔH	28427.01 J/mol	
Reaction entropy ΔS	99.52 J/mol	

It is worthwhile noticing that, activation energy, reaction constant, as well as reaction enthalpy and entropy where determined from experimental data

The physic conditions in the present simulation are listed in Table 4. Avrami exponent was determined from experimental data modeling as it was detailed below.

Table 4. Physic conditions for simulation

Properties	***Value***
Hydrogen supply pressure P_g	20 bar
Temperature T_{cool}	293K
Water velocity v	0.32m/s
Hydrogen storage capacity wt %	1.1
Avrami exponent n	0.68

4 Results anddiscussion

4.1 Gaseous phase studies

Gaseous phase hydrogen storage properties were studied by PCT measured at 298, 313, and 328 K. PCT curves were run for the studied sample at different temperatures to obtain the thermodynamic parameters involved in the hydriding process. The resulting absorption and desorption isotherms are shown in Fig. 1. and the information obtained is summarized in Table 5. The sample shows a slightly higher capacity at the lowest temperature as well as the smallest hysteresis and equilibrium pressure. Slopes of these isotherms are between the typical values obtained for AB5 MH alloys. Due to the lack of a well-defined plateau region in the isotherm, the pressure at 0.7 wt.% H-storage is used as a measure of equilibrium plateau pressure.

Hysteresis of the PCT isotherm is defined as ln (Pa/Pd), where Pa and Pd are the absorption and desorption equilibrium pressures at 0.7 wt.% H-storage. In the studied alloy, the hysteresis increases with the increase in measuring temperature. This difference may arise from the similar metal-hydrogen bond strength of the multiple superlattice phase [32]. It is worthwhile noticing that it was expected that PCT hysteresis decreases with increasing measuring temperature because less energy is required to distort the lattice during hydrogenation [33]

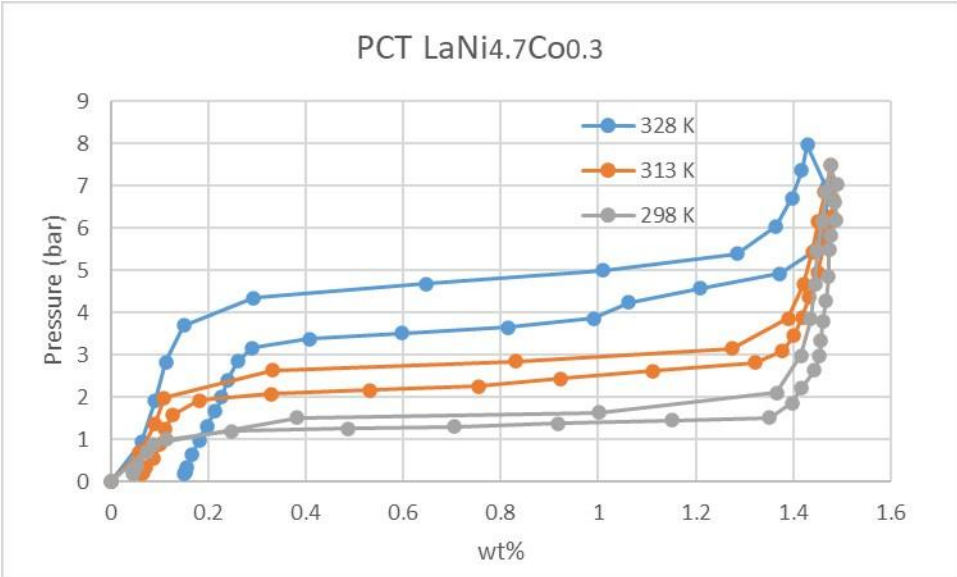

Figure 1. PCT curves for $LaNi_{4.7}Co_{0.3}$ at 298, 313 and 328K.

Table 5. Hydrogen storage capacity and Equilibrium Pressures (*Peq*) for *La* $Ni_{4.7}Co_{0.3}$ at the studied temperatures

Temperature (K)	**Capacity w%**	**P_{eq}*(bar) Absorption***	**P_{eq}*(bar) Desorption***	**Hysteresis**
298	1.48	1.6	1.4	0.13
313	1.47	2.8	2.4	0.15
328	1.42	4.7	3.5	0.29

Table 6 summarizes thermodynamic properties determinate by Van´t Hoff equation reported in Figure 2

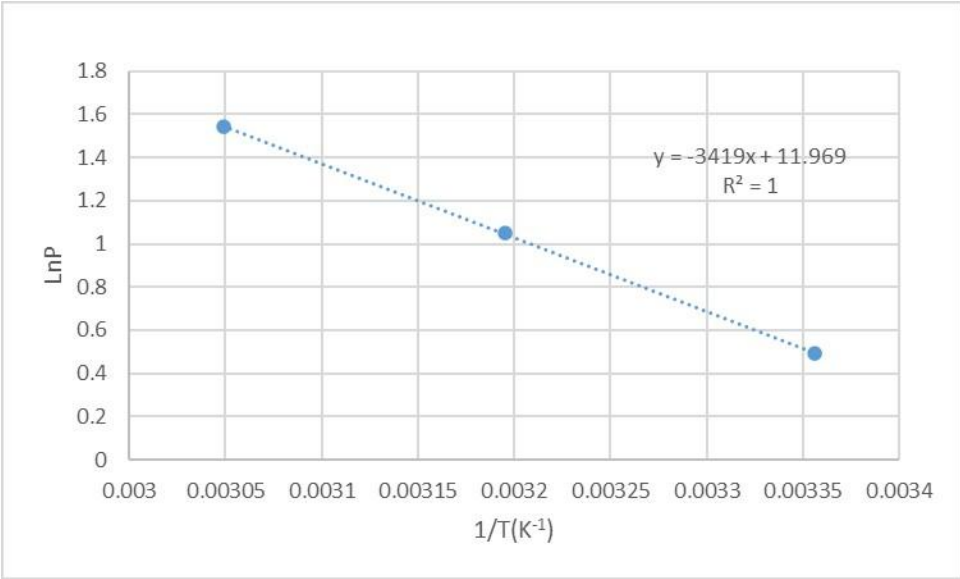

Figure 2. Graphical of Van't Hoff for the alloy *La* $Ni_{4.7}Co_{0.3}$

Table 6. $LaNi_{4.7}Co_{0.3}$ thermodynamic properties determined by Van**'**t Hoff equation

Alloy	**Slope**	**Ordinate**	***ΔH* (J/mol)**	***ΔS* (J/mol.K)**
$LaNi_{4.7}Co_{0.3}$	-3419	11.969	-28427.01	99.52

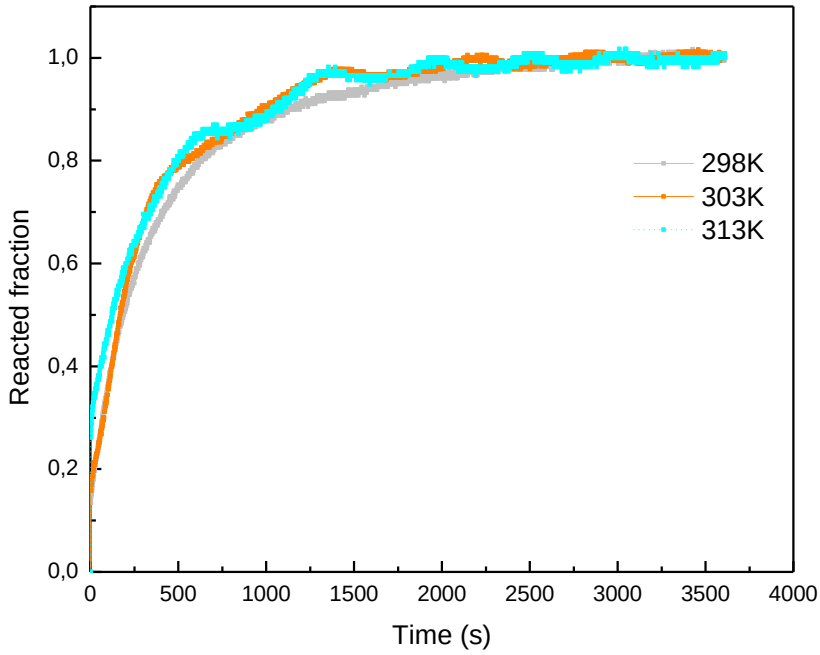

Figure 3. Fraction of absorption reaction vs time of *La Ni*4.7*Co*0.3 at different temperatures

The isothermal hydrogen absorption kinetic curves at the studied temperature are shown in Figure 3. The Johnson−Mehl−Avrami-Kolmogorov (JMAK) model was utilized to simulate the curves related to hydrogen storage kinetics and hydrogen absorption activation, and the Arrhenius method was employed to calculate the critical value. It is widely acknowledged that hydrogen absorption reactions are related to total energy barriers, which must be considered in hydrogen absorption processes. The JMAK model can be used to simulate the nucleation and growth processes of the alloys as it is expressed in equation 4:

$$\ln(-\ln(1-\xi)) = n \ln t + \ln k$$

As seen from Fig. 4, by utilizing the logarithmic transformation, we can obtain JMAK curves at 298,303 and 313K for the hydrogenation of the studied alloy.

The Avrami exponent n describes the possibility of nucleation as well as it gives information about the rate limiting step and the dimensionality of the growth process. Specifically, the Avrami exponent can be expressed as $n = \frac{d}{m} + a$, where d represents the dimensionality of the growth, a is related to the nucleation rate. When site is saturated, a =0, when the number of available nuclei decreases with time, 0< a <1. On the other hand, when the number of available nuclei increases with time, there will be increasing nucleation and a >1. Finally, when the number of available nuclei is constant a =1. Variable m reveals the mechanism of the control step, for m =1, the reaction is interface-controlled growth, and m =2 indicates diffusion-limited growth.

The ln[-ln(1-ξ)] is plotted as a function of ln t in Fig. 4, which demonstrates that the hydride develops in two stages. The reaction rate in stage 1, which takes place in a very short time is associated with n values of 0.13-0.15, these reaction orders indicate no hydride nucleation and growth (α phase).

In the stage 2, the obtained minimum value of n was 0.63. A n value smaller than 1.0 indicates that the rate limiting step is diffusion. The n value varied within a narrow range from 0.63 to 0.71; therefore, it is expected that the rate limiting step does not change within the temperature and pressure range of the experiment. The obtained n values correspond to one -dimensional grain growth with decreasing nucleation rate. The smaller n values obtained at higher temperatures suggest that the nucleation and growth of hydride is inhibited because of the rapid increase of the fraction of hydride. The absorption curves were fitted with straight lines. Arrhenius methods can be then used to calculate the Ea.

As seen from Fig 5, by utilizing the logarithmic transformation, we can obtain Arrhenius curves of ln k and 1/T at 298, 303, and 313K for the hydrogenation process. The Arrhenius curves are found to be nearly linear and Ea value can be calculated by the slope of the line. Tables 7 and 8 report values obtained after modeling.

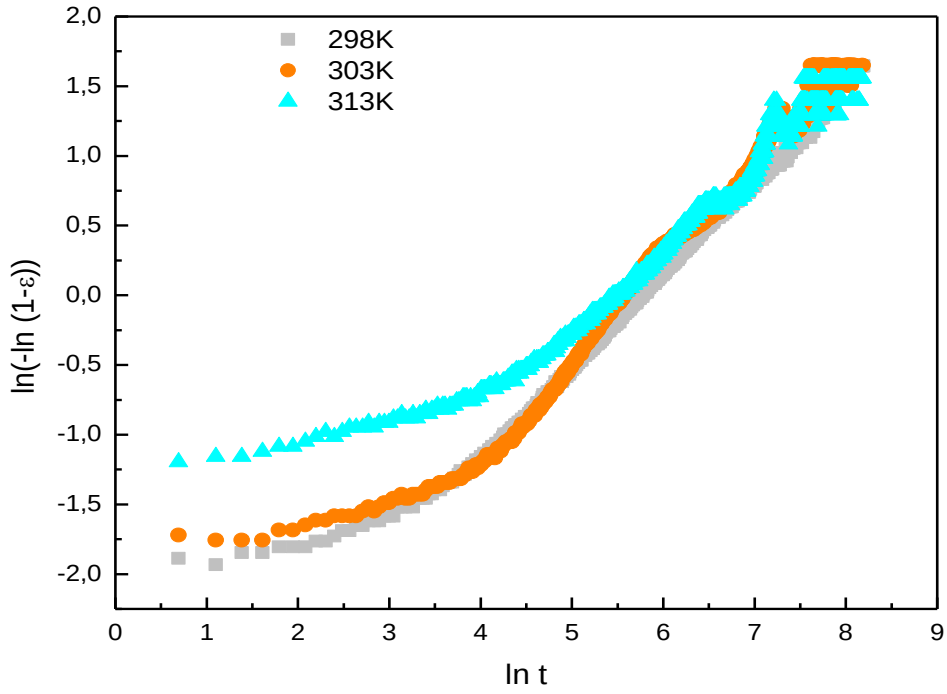

Ojo que en el grafico debe ir ξ

Figure 4. JMAK curves at 298K (grey) ,303K (orange) and 313K (light blue) for the hydrogenation of the studied alloy.

Table 7. Results obtained from kinetic adjustments in the second region.

Alloy	Temperature	n	ln *k*	k
$LaNi_{4.7}Co_{0.3}$	298	0.71	-4.12079	0.016
	303	0.69	-3.8845	0.021
	313	0.63	-3.45611	0.032

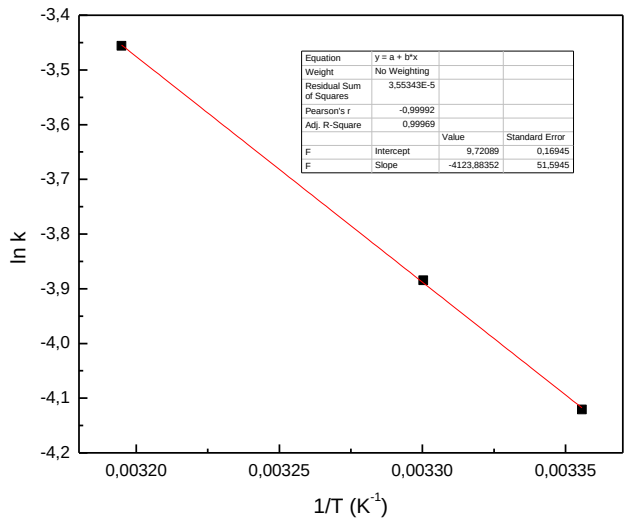

Figure 5. Arrhenius plot for *La* $Ni_{4.7}Co_{0.3}$

Table 8. Result obtained from kinetic adjustment

Alloy	Slope	Ea(kJ/mol)	$k_{iso}(s^{-1})$
$LaNi_{4.7}Co_{0.3}$	-4123.9	34.3	16662

4.2 Modeling results

Fig.6(a) displays the prediction of the mean temperature integrated on the whole volume of the cylinder with time evolution. It is observed that tank with inner cooling tube have a great drop of temperature in less than 500s. It will have a lower temperature increase than the tank without cooling system, which means it will have a higher rate of absorption. Fig.6(b) shows the temperature distribution along with the radius of these two cylinders at the time at which the average temperature reaches its maximum.

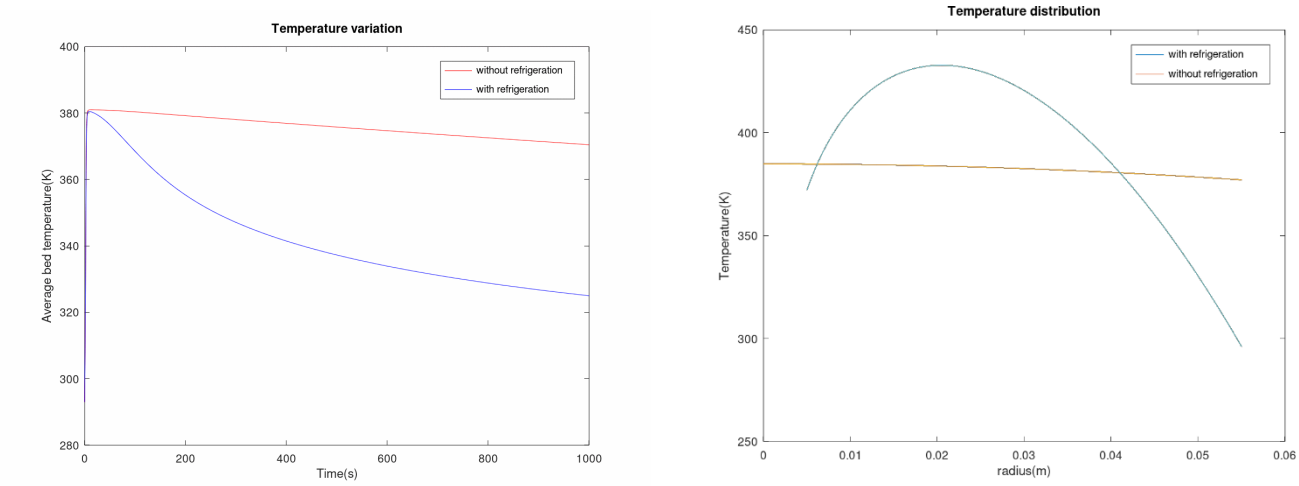

(a) Average bed temperature variation (b) Temperature distribution

Figure 6. Average bed temperature variation and temperature distribution

Fig.7 shows the temperature distribution in 3D mode when the average temperature is in the highest point.

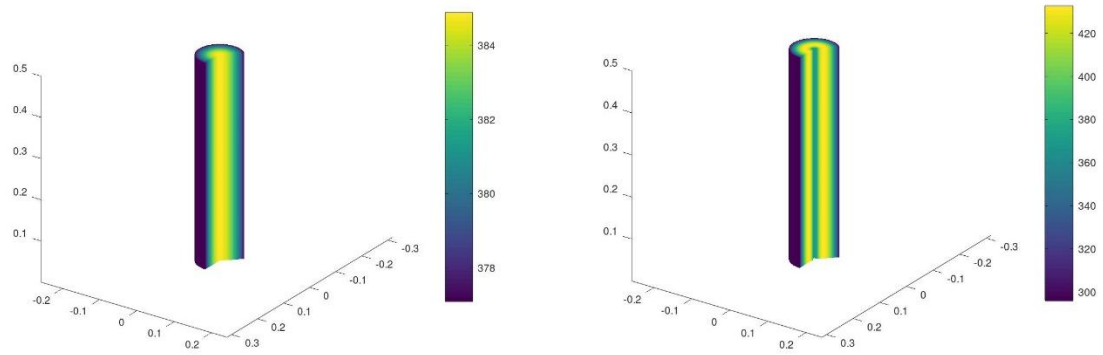

(a) Temperature distribution without inner tube (b) Temperature distribution with inner tube

Figure 7. 3D temperature distribution (a) without inner tube (b) with inner tube

Table 9. Simulation results of tank without inner tube

Simulation result	Value
Time to arrive the maximum average temperature	14 s
Fraction of reaction	0.863
Equilibrium pressure	19.988 bar
Global heat transfer coefficient U	6.1421W/m^2s
Mass rate of hydrogen absorption	1.159 g/m^3 s
Average temperature	381 K

Maximum temperature	384.89 K
Surface temperature	377.1 K

Table 10. Simulation results of tank with inner tube

Simulation result	Value
Time to arrive the maximum average temperature	10 s
Fraction of reaction	0.7899
Equilibrium pressure	19.765bar
Global heat transfer coefficient U	1932.6W/m_2s
Mass rate of hydrogen absorption	34.654 g/m^3
Average temperature	380.52 K
Maximum temperature	432.81 K
Position of maximum temperature r_m	0.0205 mm
Inner tube Surface temperature T_{s_1}	372.11 K
Surface temperature T_{s_2}	2 96.07K

Tables 9 and 10 depict numerical results for times when the average temperature of tanks is maximum. It shows that the mass rate of hydrogen in tanks with inner tube is faster than the condition for tanks without inner tube. Even though the maximum temperature of tank with refrigeration is higher than the one without an inner tube, the average temperature is slightly lower. Thus, the equilibrium pressure in the refrigerated tank is lower than the unrefrigerated one. From the numerical prediction the tank with refrigeration will faster arrive to the maximum temperature.

Fig.9 shows the effect of supply pressure. Increasing of the supply pressure has a rise of cylinder temperature, because of the faster absorption rate. Due to this increase of temperature, the equilibrium pressure also increases, which drives the decreases of the potential and absorption rate.

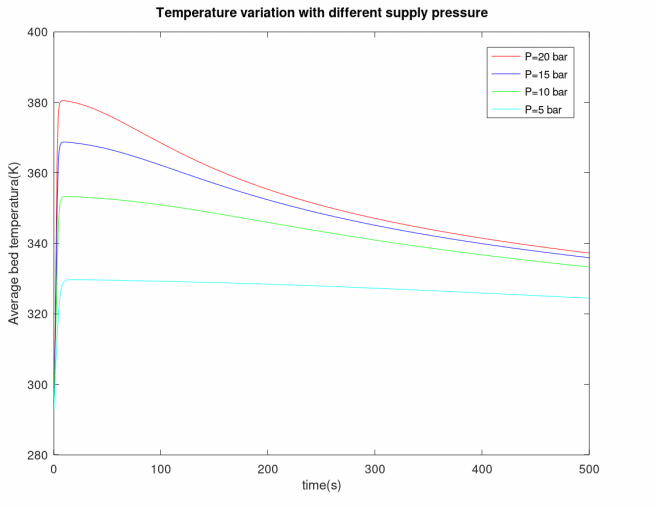

Figure 9. Temperature variation with different supply pressure for the tank with inner tube

5. Conclusions

A 3D numerical model has been developed using the software Octave for predicting the performance of a metal hydride tank filled with LaNi4.7Co0.3 alloy. Hydrogen storage properties were studied by PCT measured at 298, 313, and 328 K to obtain the thermodynamic parameters involved in the hydriding process.

The Johnson−Mehl−Avrami-Kolmogorov (JMAK) modeled hydrogen storage kinetics and hydrogen absorption activation. The obtained reaction orders values correspond to one -dimensional grain growth with decreasing nucleation rate.

The model can be used as a useful method to evaluate the metal-hydrogen reactor as well as metal hydride performances optimizing designs.

Acknowledgments

Authors acknowledge CSIC-UdelaR, PEDECIBA and ANII. C.Z., E.T., and V.D. are researchers at PEDECIBA/United Nations

References

[1] B. Nastasi, G.L. Basso, Hydrogen to link heat and electricity in the transition towards future Smart Energy Systems, Energy 110 (2016) 5–22.

[2] G. Gahleitner, Hydrogen from renewable electricity: an international review of power-to-gas pilot plants for stationary applications, Int. J. Hydrogen Energy 38 (2013) 2039–2061.

[3] R.B. Olsen, Hydrogen metal-hydride thermal to electrical conversion: hymtec, Energy 11 (1986) 869–871.

[4] S. S. Bhogilla. “Design of a AB2-metal hydride cylindrical tank for renewable energy storage”. J. Energy Storage 14 (2017), pp. 203–210.

[5] C. Darras, M. Muselli, P. Poggi, C. Voyant, J.C. Hoguet, F. Montignac, PV output power fluctuations smoothing: the MYRTE platform experience, Int. J. Hydrogen Energy 37 (2012) 14015–14025.

[6] B.S. Sekhar, H. Ito, A. Kato, A. Nakano, Research and development of a laboratory scale totalized hydrogen energy utilization system, Int. J. Hydrogen Energy 41 (2016) 1224–1236.

[7] M. Paskevicius, D.A. Sheppard, K. Williamson, C.E. Buckley, Metal hydride thermal heat storage prototype for concentrating solar thermal power, Energy 88 (2015) 469–477.

[8] R.E. Clarke, S. Giddeya, F.T. Ciacchi, S.P.S. Badwala, B. Paul, J. Andrews, Direct coupling of an electrolyser to a solar PV system for generating hydrogen, Int. J. Hydrogen Energy 34 (2009) 2531–2542

[9] A. Nakano; T. Maeda; H. Ito; M. Masuda; Y. Kawakami; A. Kato; M. Tange; T. Takahashi; M. Matsuo. “Small-scale hydrogen liquefaction with a two-stage Gifford-McMahon cycle refrigerator”, Int. J. Hydrogen Energy 35.9088–9094 (2010).
[10] M.V. Lototsky V.A. Yartys. “An overview of hydrogen storage methods”, Phys. Chem 172.75–104 (2005).
[11] Zuttel A.Schlapbach L.Borgschulte A.Ed. John Wiley & Sons. Hydrogen as an Energy Carrier. International series of mono- graphs on physics. Inc, 2005.
[12] Kaplan Y, Veziroglou TN. Mathematical modelling of hydrogen storage in LaNi5 hydride bed. Int J Hydrogen Energy 2003;27:1027–38.
[13] M.V. Lototskyy; B.S. Sekhar; P. Muthukumar; V. Linkov; B.G. Pollet. “Niche applications of metal hydrides and related thermal management issues”, J. Alloys Compd 645.S117–22 (2015).
[14] E.S. Kikkinides; M.C. Georgiadis; A.K. Stubos. “Dynamic modelling and optimization of hydrogen storage in metal hydride beds”, Energy 31.2428–2446 (2006).
[15] S.S. Mohammadshahi; E.MacA. Gray; C.J. Webb. “A review of mathematical modelling of metal hydride systems for hydrogen storage applications”, International Journal of Hydrogen Energy 15 (2015).
[16] M. Groll, U. Mayer, W. Supper. “Heat and mass transfer in metal hydride reaction beds: experimental and theoretical results”. Journal of the Less-Common Metals 131.1987 (1986), pp. 235–244.
[17] Jemni A, Nasrallah SB. Study of two-dimensional heat and mass transfer during absorption in a metal-hydrogen reactor. Int J Hydrogen Energy 1995;20(1):43–52.
[18] Nasrallah SB, Jemni A. Study of two-dimensional heat and mass transfer during desorption in a metal-hydrogen reactor. Int J Hydrogen Energy 1997;22(1):67–76.
[19] Jemni A, Nasrallah B, Lamloumi J. Experimental and theoretical study of a metal-hydrogen reactor. Int J Hydrogen Energy 1999;24:631–44.
[20] Nakagawa T, Inomata A, Aoki H, Miura T. Numerical analysis of heat and mass transfer characteristics in the metal hydride bed. Int J Hydrogen Energy 2000;25:339–50.
[21] Askri F, Jemni A, Nasrallah SB. Study of two-dimensional and dynamic heat and mass transfer in a metal-hydrogen reactor. Int J Hydrogen Energy 2003;28:537–57.
[22] Mat MD, Kaplan Y. Numerical study of hydrogen absorption in an La–Ni5 hydride reactor. Int J Hydrogen Energy 2001;26:957–63.
[23] Aldas K, Mat MD, Kaplan Y. A three-dimensional model for absorption in a metal hydride bed. Int J Hydrogen Energy 2002;27:1049–56.
[24] Mat MD, Kaplan Y, Aldas K. Investigation of three-dimensional heat and mass transfer in a metal hydride reactor. Int J Energy Res 2002;26:973–86.
[25] Evangelos I. Gkanas, Martin Khzouz, Renewable Energy, 2017; 111:484-493

[26] Qian Li Yuepeng Pang. “A review on kinetic models and corresponding analysis methods for hydrogen storage materials”. Int. J. Hydrog. Energy 4I.40 (2016), pp. I8072–I8087.
[27] Philippe Marty. J-F.Fourmigue. P.De Rango. D.Fruchart. J.Charbonnier. “Numerical simulation of heat and mass transfer during the absorption of hydrogen in a magnesium hydride”. Elsevier 47.2006 (2006), pp. 3632–3643.
[28] Raquel Busqué. Ricardo Torres. Joan Grau. Vicente Roda. Attila Husar. “Mathematical modeling, numerical simulation and experimental comparison of the desorption process in a metal hydride hydrogen storage system”. International Journal of Hydrogen Energy, 43 (2018) pp 16929-16940
[29] T. L. Bergman; A. S. Lavine; F. P. Incropera; D.P. DewittT. Fundamentals of Heat and Mass Transfer. Seven Edition. John Wiley & Sons, Inc, 2011.
[30] Churchill; S. W.; and H. H. S. Chu. “Heat Mass Transfer”. In: Int. J. Vol.18 (1975)
[31] James O. Maloney Robert H. Perry Don W. Green. Perry Chemical Engineers Handbook. SEVENTH EDITION. The McGraw Hill Companies, 199
[32] K. Young, T. Ouchi, B. Huang, B. Reichman, R. Blankenship, J. Alloys Compd. 575 (2013) 65-72.
[33] K. Young, D.F. Wong, L. Wang , J. Nei, T. Ouchi , S. Yasuoka, Journal of Power Sources 218 (2012) 487-494